

Loop induced top quark FCNC through top quark and dark matter interactions

Yandong Liu,^{1,2,*} Bin Yan,^{3,†} and Rui Zhang^{4,‡}

¹Key Laboratory of Beam Technology of Ministry of Education,
College of Nuclear Science and Technology, Beijing Normal University, Beijing 100875, China

²Beijing Radiation Center, Beijing 100875, China

³Theoretical Division, Group T-2, MS B283, Los Alamos National Laboratory, P.O. Box 1663, Los Alamos, NM 87545, USA

⁴Theoretical Physics Division, Institute of High Energy Physics, Beijing 100049, China

We present a comprehensive analysis of the loop induced top quark FCNC signals at the LHC within one class of the simplified model. The loop level FCNC interactions are well motivated to avoid the hierarchy of the top quark couplings from the new physics and standard model. Such a theory will posit a Majorana dark matter candidate and could be tested through dark matter relic density, direct detection experiments (the scattering between dark matter and heavy nuclei), and the collider signals at the LHC. We find that the spin-independent (SI) scattering between Majorana dark matter and nuclei will vanish at the leading order, while the next-to-leading order correction to the SI scattering becomes significant to constrain the parameter space of the model. A detailed comparison between direct detection experiments and LHC searches is also discussed and both of them are very important to fully constrain the model.

I. INTRODUCTION

Top quark flavor changing neutral current (FCNC) processes can only occur via loops in the standard model (SM) and their production rates are highly suppressed by the Glashow-Iliopoulos-Maiani mechanism [1]. For example, the branching ratios of top quark decay $t \rightarrow Xq$, where $X = h, Z, \gamma, g$ and $q = u, c$ are around $10^{-16} \sim 10^{-12}$ in the SM [2]. As a result, it would be a challenge to observe the SM top quark FCNC effects with the current or foreseeable dataset. However, the testable top quark FCNC signals could be induced in the new physics (NP) beyond the SM at the tree or loop level, e.g. $\text{BR}(t \rightarrow Xq) \sim \mathcal{O}(10^{-5})$ in the minimal supersymmetry standard model (MSSM) [2] or two Higgs doublet model [3–5]. Therefore, any evidence of the top quark FCNC signals would shed light on the various possible NP models and also the underlying mechanism of generating top quark FCNC.

The top quark FCNC effects have been extensively studied by the theoretical [6–19] and experimental [20–35] groups within the SM effective field theory (SMEFT) framework or specific NP models. Both the ATLAS and CMS collaborations show that the current dataset could put a strong constraint on the $\text{BR}(t \rightarrow Xq)$ through top quark rare decay and single top quark production. For example, the most stringent limits on the branching ratios of $\text{BR}(t \rightarrow \gamma u) < 6.1 \times 10^{-5}$ and $\text{BR}(t \rightarrow \gamma c) < 2.2 \times 10^{-4}$ at the 95% confidence level (CL) are set by the single top quark and a photon production [21] at the 13 TeV LHC. The limit of the $\text{BR}(t \rightarrow gq)$ is comparable to the $\text{BR}(t \rightarrow \gamma q)$ and it shows that the upper limit is 2×10^{-5} and 2×10^{-4} for u and c quark,

respectively at the LHC Run-I [23, 24]. Both the top quark decay [23, 24, 33, 35] and single top quark associated with a gauge boson production [28, 34] could constrain the branching ratios $\text{BR}(t \rightarrow Z/hq)$ and the most stringent limits come from the top quark decay, i.e. $\text{BR}(t \rightarrow Zu) < 1.7 \times 10^{-4}$, $\text{BR}(t \rightarrow Zc) < 2.4 \times 10^{-4}$, $\text{BR}(t \rightarrow hu) < 1.1 \times 10^{-3}$ and $\text{BR}(t \rightarrow hc) < 1.2 \times 10^{-3}$.

The SMEFT is a powerful framework to parametrize potential NP effects and widely applied in the top quark FCNC phenomenology [36–38]. The corresponding Wilson coefficients are constrained to be around $\mathcal{O}(10^{-3}) \sim \mathcal{O}(10^{-2})$ with the NP scale $\Lambda = 1$ TeV. With higher luminosity data being accumulated, an order of magnitude improvement on the top quark FCNC anomalous couplings is expected at the high-luminosity LHC (HL-LHC), operating at the $\sqrt{s} = 14$ TeV with an integrated luminosity of 3 ab^{-1} . Thus it is timely to check those NP models which could induce the top quark FCNC anomalous couplings.

The top quark FCNC anomalous couplings could be generated through the tree or loop level in NP models. It is well known that the multiplet Higgs models could generate tree level top quark FCNC couplings if the Yukawa structure violates the Glashow-Weinberg-Paschos (GWP) theorem [39, 40], e.g. the general two Higgs double models. However, such models have been constrained seriously by top quark FCNC data, and as a result, a large hierarchy was generated between top quark FCNC and other top quark couplings (e.g. tbW [41, 42] and $Zt\bar{t}$ [43]). This situation could be relaxed or avoided if we require the top quark FCNC couplings to be generated only in the loop level, which is similar to the case of the loop induced neutrino mass models [44, 45]. For example, the top quark FCNC couplings could be generated by triangle loop diagram through the squarks mixing effects in the MSSM and its value agrees well with the LHC limitation as the mass scale of $\mathcal{O}(1)$ TeV for the heavy particles in the loop, without unduly small NP couplings.

One obvious way of generating loop induced top quark

* ydliu@bnu.edu.cn

† binyan@lanl.gov

‡ zhangr@ihep.ac.cn

FCNC couplings is introducing an additional \mathcal{Z}_2 symmetry to avoid possible tree level interactions, i.e. new heavy particles are odd under the \mathcal{Z}_2 , while the SM particles are even. One byproduct of such models is that the lightest \mathcal{Z}_2 odd neutral particle could be a promising dark matter (DM) candidate. Therefore, it is useful to combine dark matter direct detection and the collider searches to constrain or search this kind of the NP models. Comparing to the UV complete theories such as MSSM, we would like to use a simplified model to show the idea in this work. The simplified models include a finite number of parameters with a reasonable simple theoretical framework and have become a robust mechanism to search various NP particles. In this work, we will focus on the fermionic dark matter and scalar mediators. It is also possible to introduce a dark gauge boson in the loop, however, which is beyond the scope of this work. We show that the simplified model could generate the sizable top quark FCNC anomalous couplings and their predictions are consistent with the present LHC data and could be tested at the HL-LHC and future hadron colliders. In addition, the parameter space is also testable by the future dark matter direct detection experiments, (e.g. XENON20T [46] and DARWIN [47]) and dark matter searches at the LHC.

II. MODEL SETUP

In this section, we discuss the detail of our simplified model. It contains a fermionic dark matter (χ) and scalar mediator particles which interact with the dark matter and the SM quarks. The dark matter is a singlet under the SM gauge groups and can be either a Dirac or a Majorana fermion and we will focus on the Majorana case in this work. In general, the top quark from the NP interactions could be both left and right-handed under the $SU(2)_L$ gauge symmetry. However, the left-handed top and bottom quarks transform as doublet under $SU(2)_L$, and as a result, any modification to the left-handed top quark couplings will also induce corrections to B physics, e.g. [48, 49]. Therefore, we will focus on the right-handed top quark case in order to avoid the possible constraints from precise measurements of B physics. The gauge representations of the mediators under the SM gauge group $SU(3)_C \otimes SU(2)_L \otimes U(1)_Y$ are,

$$\Phi_1 \sim (3, 1, 2/3), \quad \Phi_2 \sim (3, 2, 1/6). \quad (1)$$

The general gauge invariant Lagrangian can be written as following

$$\begin{aligned} \mathcal{L}_{\text{eff}} \supset & (D_\mu \Phi_1)^\dagger (D^\mu \Phi_1) + (D_\mu \Phi_2)^\dagger (D^\mu \Phi_2) - M_2^2 \Phi_2^\dagger \Phi_2 \\ & - M_1^2 \Phi_1^\dagger \Phi_1 + (Y_{RI} \bar{\chi} P_R U_I \Phi_1^* + Y_{LI} \bar{Q}_I P_R \chi \Phi_2 + \text{h.c.}) \\ & + \frac{1}{2} \bar{\chi} (\not{\partial} - m_\chi) \chi - (\mu \Phi_1^* H \Phi_2 + \text{h.c.}) + \dots, \end{aligned} \quad (2)$$

where U_I and Q_I are the right- and left-handed quarks under $SU(2)_L$ with the family index $I = 1, 2, 3$, respectively. H is the Higgs doublet field and defined as

$H^T = \frac{1}{\sqrt{2}}(0, v + h)$ with $v = 246$ GeV in the unitarity gauge. The covariant derivative in Eq. 2 is defined as,

$$D_\mu = \partial_\mu - ig_s G_\mu^a T^a - ig W_\mu^i \tau^i - ig' Y B_\mu. \quad (3)$$

Here G_μ^a , W_μ^i and B_μ are the $SU(3)_c$, $SU(2)_L$ and $U(1)_Y$ gauge fields, respectively, and g_s , g and g' are their gauge couplings. The gauge parameters g and g' are related to the electric charge and the Weinberg mixing angle by $gs_W = g'c_W = e$, where $s_W = \sin \theta_W$ and $c_W = \cos \theta_W$. Furthermore, T^a and τ^i are the $SU(3)_c$ and $SU(2)_L$ generators and Y is the hypercharge, in the representation of the field on which the derivative acts.

After the electroweak symmetry breaking, we should introduce quark transform matrices ($V^{R,L}$) in the Yukawa sector of the new mediators due to the misalignment of the weak and mass eigenstate of the quarks in the SM, i.e.

$$\mathcal{L}_{\text{Yukawa}} = Y_{RI} V_{Ii}^R \bar{\chi} P_R u_i \Phi_1^* + Y_{LI} V_{Ii}^L \bar{q}_i P_R \chi \Phi_2 + \text{h.c.} \quad (4)$$

To avoid the possible limits from the low energy data, the maximal flavor violating assumption [50, 51] will be used in the analysis. Such ansatz could be realized through some flavor symmetry assumption [52] or some turning of the underlying model parameters. Here, we will not restrict ourselves to any underlying model, and instead take a phenomenological approach towards the maxima flavor violation case. The effective Yukawa couplings which are related to the top quark FCNC anomalous couplings could be parametrized as,

$$\mathcal{L}_{\text{Yukawa}} = y_t \bar{\chi} P_R t \Phi_1^* + y_u \bar{q}_u P_R \chi \Phi_2 + \text{h.c.}, \quad (5)$$

where t and $q_u^T = (u, d)$ are the right-handed top quark and left-handed first generation quarks, respectively. It is straightforward to generalize our results to the second generation light quarks. A similar simplified model with other assumptions are also widely discussed in the literature and could be found in Refs. [53–55].

After the electroweak symmetry breaking, the colored doublet scalar $\Phi_2^T = (\phi_u, \phi_d)$ will mix with Φ_1 through the 3-scalar interaction. We define the mass eigenstates as ϕ_1, ϕ_2 which can relate to the gauge eigenstates by

$$\begin{pmatrix} \phi_1 \\ \phi_2 \end{pmatrix} = \begin{pmatrix} \cos \theta & -\sin \theta \\ \sin \theta & \cos \theta \end{pmatrix} \begin{pmatrix} \Phi_1 \\ \phi_u \end{pmatrix}. \quad (6)$$

The mixing angle θ is defined as

$$\sin 2\theta = \frac{\sqrt{2}\mu v}{m_2^2 - m_1^2}, \quad (7)$$

where $m_{1,2}$ are the mass of the two physics scalars,

$$m_1^2 = \frac{1}{2}(M_1^2 + M_2^2 - \sqrt{(M_1^2 - M_2^2)^2 + 2\mu^2 v^2}), \quad (8)$$

$$m_2^2 = \frac{1}{2}(M_1^2 + M_2^2 + \sqrt{(M_1^2 - M_2^2)^2 + 2\mu^2 v^2}). \quad (9)$$

The mass of scalar ϕ_d is same as M_2 and can be related to the $m_{1,2}$ by

$$M_2^2 = m_2^2 \cos^2 \theta + m_1^2 \sin^2 \theta. \quad (10)$$

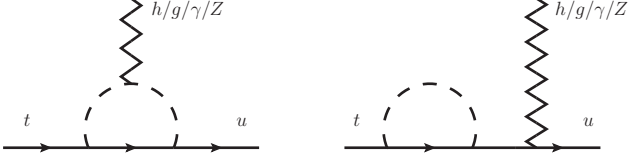


FIG. 1. Illustrative one-loop Feynman diagrams to generate top quark FCNC anomalous couplings. The left diagram depicts the vertex correction and the right one is corresponding to the quark field mixing.

III. LOOP INDUCED TOP QUARK FCNC

The top quark FCNC anomalous couplings could be generated through the triangle and self-energy diagrams in our simplified model; see Fig. 1. And the interactions can be parameterized by the effective operators under the $SU(3)_C \otimes U(1)_{EM}$:

$$\mathcal{L}_{\text{eff}} = \lambda_{tqh} \bar{q}_L t_R h + \frac{\lambda_{tq\gamma}}{m_t} \bar{q}_L \sigma_{\mu\nu} t_R A^{\mu\nu} + \frac{\lambda_{tqg}}{m_t} \bar{q}_L \sigma_{\mu\nu} t_R G^{\mu\nu} T^a + \frac{\lambda_{tqZ}^{(1)}}{m_t} \bar{q}_L \sigma_{\mu\nu} t_R Z^{\mu\nu} + \lambda_{tqZ}^{(2)} \bar{q}_L \gamma_\mu t_L Z^\mu + h.c.. \quad (11)$$

Note that the gauge invariance of $U(1)_{EM}$ forbids the vector and axial-vector current interactions of $tq\gamma$ and tqg . The matching coefficients could be obtained from one-loop calculations and the results are,

$$\lambda_{tqh} = \frac{y_t y_u m_\chi}{16\sqrt{2}\pi^2} \left\{ \frac{\sin 2\theta}{\sqrt{2}v} (B_{\chi 1}^0 - B_{\chi 2}^0) + \mu (\sin^4 \theta - \sin^2 \theta \cos^2 \theta) C_{\chi 12}^{0ht} + \mu (\cos^4 \theta - \sin^2 \theta \cos^2 \theta) C_{\chi 21}^{0ht} + 2\mu \sin^2 \theta \cos^2 \theta C_{\chi 11}^{0ht} + 2\mu \sin^2 \theta \cos^2 \theta C_{\chi 22}^{0ht} \right\}, \quad (12)$$

$$\lambda_{tq\gamma} = \frac{Qe}{32\pi^2} \frac{m_\chi}{m_t} y_t y_u \sin \theta \cos \theta (B_{\chi 2}^t - B_{\chi 2}^0 - B_{\chi 1}^t + B_{\chi 1}^0), \quad (13)$$

$$\lambda_{tqg} = \frac{g_s}{32\pi^2} \frac{m_\chi}{m_t} y_t y_u \sin \theta \cos \theta (B_{\chi 2}^t - B_{\chi 2}^0 - B_{\chi 1}^t + B_{\chi 1}^0), \quad (14)$$

$$\begin{aligned} \lambda_{tqZ}^{(1)} = & \frac{g}{16\pi^2 c_W} \frac{m_\chi m_t}{4(m_t^2 - m_Z^2)} y_t y_u \sin 2\theta \left\{ (B_{\chi 1}^0 - B_{\chi 2}^0) f_R - \frac{m_t^2 + m_Z^2}{m_t^2 - m_Z^2} f_L (B_{\chi 1}^t - B_{\chi 2}^t) \right. \\ & + \frac{m_Z^2}{m_t^2 - m_Z^2} [(2f_L - \cos^2 \theta) B_{11}^Z - (2f_L - \sin^2 \theta) B_{22}^Z + \cos 2\theta B_{12}^Z] \\ & + \frac{m_Z^2}{2(m_t^2 - m_Z^2)} [(2f_L - \cos^2 \theta) \lambda(m_1) C_{1\chi 1}^{0tZ} - (2f_L - \sin^2 \theta) \lambda(m_2) C_{2\chi 2}^{0tZ}] \\ & + \frac{\cos^2 \theta}{4(m_t^2 - m_Z^2)} [2(m_1^2 - m_2^2) m_t^2 + (\lambda(m_1) + \lambda(m_2)) m_Z^2] C_{2\chi 1}^{0tZ} \\ & \left. + \frac{\sin^2 \theta}{4(m_t^2 - m_Z^2)} [2(m_1^2 - m_2^2) m_t^2 - (\lambda(m_1) + \lambda(m_2)) m_Z^2] C_{1\chi 2}^{0tZ} \right\} \end{aligned} \quad (15)$$

$$\lambda_{tqZ}^{(2)} = -\frac{g}{16\pi^2 c_W} \frac{m_\chi}{m_t} y_t y_u f_L \sin \theta \cos \theta (B_{\chi 2}^t - B_{\chi 2}^0 - B_{\chi 1}^t + B_{\chi 1}^0) + 2\lambda_{tqZ}^{(1)}. \quad (16)$$

where

$$f_L = \frac{1}{2} - \frac{2}{3} s_W^2, \quad f_R = -\frac{2}{3} s_W^2, \quad \lambda(m_i) = 2m_\chi^2 - 2m_i^2 - m_t^2 + m_Z^2. \quad (17)$$

We abbreviate the scalar functions as $B_{ij}^a = B_0(m_a^2, m_i^2, m_j^2)$ and $C_{ijk}^{abc} = C_0(m_a^2, m_b^2, m_c^2, m_i^2, m_j^2, m_k^2)$, and their definitions can be found in Ref. [56]. Note that $m_{a,b,c} = 0$ for $a, b, c = 0$.

The matching coefficients could be much simplified in

the decouple limit, i.e. $m_{1,2,\chi} \sim \Lambda \gg m_{t,h,Z}$,

$$\lambda_{tqh} \simeq -\frac{1}{384\sqrt{2}\pi^2} y_t y_u \mu \frac{m_t^2}{\Lambda^3}, \quad (18)$$

$$\lambda_{tq\gamma} \simeq \frac{iQe}{392\sqrt{2}\pi^2} y_t y_u \frac{\mu v m_t}{\Lambda^3}, \quad (19)$$

$$\lambda_{tqg} \simeq \frac{ig_s}{392\sqrt{2}\pi^2} y_t y_u \frac{\mu v m_t}{\Lambda^3}, \quad (20)$$

$$\lambda_{tqZ}^{(1)} \simeq -\frac{gy_t y_u (f_L + f_R)}{768\sqrt{2}\pi^2 c_W} \frac{\mu v m_t}{\Lambda^3}, \quad (21)$$

$$\lambda_{tqZ}^{(2)} \simeq \frac{gy_t y_u (f_L - f_R)}{384\sqrt{2}\pi^2 c_W} \frac{\mu v m_t}{\Lambda^3}. \quad (22)$$

We should note that the scale $\mu \sim v$ in above limit, see Eq. 7.

It is also worth noting that the coefficient λ_{tqh} could be enhanced by the triple scalar interaction in a large μ limit (see Eq. 18), which could be generated by a large mass splitting between ϕ_1 and ϕ_2 for a fixed mixing angle θ . Therefore, it is interesting to consider the limit of $m_2 \gg m_{1,\chi} \sim m_{t,h,Z}$ with a fixed mixing angle θ . It shows that the coefficients could be

$$\lambda_{tqh} \simeq -\frac{13y_u y_t m_2^2 \sin^3 2\theta}{1536\pi^2 m_\chi v}, \quad (23)$$

$$\lambda_{tq\gamma} \simeq -\frac{y_u y_t Q e (2 - \pi/\sqrt{3}) \sin 2\theta}{32\pi^2}, \quad (24)$$

$$\lambda_{tqg} \simeq -\frac{y_u y_t g_s (2 - \pi/\sqrt{3}) \sin 2\theta}{32\pi^2}. \quad (25)$$

It is evident that λ_{tqh} will be enhanced by the mass m_2 , while the other coefficients ($\lambda_{tq\gamma/g/Z}$) approach a constant for a large m_2 . The result for λ_{tqZ} is still complicated in this limit and will not be shown in here.

The partial decay widths of top quark through the FCNC anomalous couplings are

$$\Gamma(t \rightarrow qh) = \lambda_{tqh}^2 \frac{m_t}{32\pi} \left(1 - \frac{m_h^2}{m_t^2}\right)^2, \quad (26)$$

$$\Gamma(t \rightarrow q\gamma) = \lambda_{tq\gamma}^2 \frac{m_t}{4\pi}, \quad (27)$$

$$\Gamma(t \rightarrow qg) = \lambda_{tqg}^2 \frac{m_t}{4\pi} 4C_F, \quad (28)$$

$$\Gamma(t \rightarrow qZ) = \frac{m_t}{32\pi} \left(1 - \frac{m_Z^2}{m_t^2}\right)^2 \left[4 \left(\lambda_{tqZ}^{(1)} \right)^2 \left(2 + \frac{m_Z^2}{m_t^2} \right) - 12 \lambda_{tqZ}^{(1)} \lambda_{tqZ}^{(2)} + \left(\lambda_{tqZ}^{(2)} \right)^2 \left(2 + \frac{m_t^2}{m_Z^2} \right) \right]. \quad (29)$$

Figure 2 shows the decay branching ratios from the top quark FCNC anomalous couplings with the benchmark parameters, namely $m_\chi = 300$ GeV, $\theta = \pi/4$, $y_u = 1.0$ and $y_t = 1.5$. The Wilson coefficients $\lambda_{tqh/\gamma/g/Z}$ can be found in Eqs. 18-16 and are calculated by LoopTools [57]. Figure 2(a) displays the top quark FCNC decay branching ratios as a function of mixing angle θ with scalar mass of $m_1 = 800$ GeV and $m_2 = 2000$ GeV. It is evident that the branching ratios will reach the maximal when the mixing angle $\theta \sim \pi/4$. This is because those top quark FCNC couplings (see Eqs. 18-16) could be generated only through the mixing between ϕ_1 and ϕ_2 , and, as a result, the maximal mixing of $\theta = \pi/4$ will induce the largest FCNC couplings. The typical branching ratios of $t \rightarrow q + Z/\gamma/g$ are around $\mathcal{O}(10^{-9}) - \mathcal{O}(10^{-8})$. However, the $\text{BR}(t \rightarrow qh)$ could be reached around $\mathcal{O}(10^{-5})$ due to the λ_{tqh} will be enhanced by m_2^2 in the limit of $m_2 \gg m_1$; see Eq. 23. Figure 2(b) depicts the top quark FCNC decay branching ratios as a function of m_2 . It is evident that $\text{BR}(t \rightarrow qh)$ is strongly dependent on the m_2 , but $\text{BR}(t \rightarrow q\gamma/g/Z)$ are not in a large m_2 region, as argued before; see Eqs. 23-25. In the limit of $m_2 \gg m_1$,

the $\text{BR}(t \rightarrow qh)$ could be around $\mathcal{O}(10^{-5})$, which is large enough and can be detected at the HL-LHC and future hadron colliders. However, it would be a challenge to probe other top quark FCNC signals of this model due to the small decay branch ratios.

Figure 3 displays the testable parameter space in the plane of the model parameters at the 95% C.L. from tqh measurement at the HL-LHC (red) [58, 59], HE-LHC (blue) [60] and FCC-HH (gray) [60]. From Fig. 3(a), it is clear that a larger m_2 will enhance the loop contribution to $t \rightarrow qh$. The contour behavior of Fig. 3(b) arises from the fact that the $\lambda_{tqh} \propto y_u y_t$. We also note that a small m_χ will weaken the loop contribution to $t \rightarrow qh$, while a moderate m_χ will result in a larger $\text{BR}(t \rightarrow qh)$; see Fig. 3(c).

We notice that the scale μ will be constrained by the unitarity of the scattering $\phi_i \phi_j^* \rightarrow W_L^+ W_L^-$ ($i, j = 1, 2$), with longitudinal polarized W boson. Based on the analysis of the partial wave expansion [61], for the s -wave,

$$a = \frac{1}{64\pi^2} \int d\Omega \mathcal{M}(\phi_i \phi_j^* \rightarrow W_L W_L), \quad (30)$$

and the coupled matrix is

$$a = \begin{pmatrix} 0 & \frac{\sqrt{2}\mu\delta_{m,n}}{32\pi v} \\ -\frac{\sqrt{2}\mu\delta_{m,n}}{32\pi v} & 0 \end{pmatrix}, \quad (31)$$

where $\delta_{m,n}$ is the color index. The unitarity of the scattering amplitude requires that the absolute value of the eigenvalues from above coupled matrix should be small than 1 [61–64]. Therefore, the upper limit of μ is

$$|\mu| \lesssim 17 \text{ TeV}. \quad (32)$$

We can also translate the upper limit of μ to the mass splitting between ϕ_1 and ϕ_2 through Eq. 7; see the black line in Fig. 3. We should note that the unitarity bound would be stronger than the limit from HL-LHC in some parameter space.

IV. DARK MATTER

In this section we discuss the constraints from the DM relic abundance and the direct detection experiments on our simplified model.

A. relic density

The DM relic abundance has been measured by Planck with a high accuracy, i.e. $\Omega_\chi h^2 = 0.1200 \pm 0.0012$ [65]. It requires that the theoretical predicted relic abundance from the simplified model should be smaller than the observed value to avoid dark matter overproduction. Assuming DM particle is thermally produced in the early universe, $\Omega_\chi h^2$ is totally determined by the thermally averaged annihilation cross sections $\langle \sigma v_{\text{rel}} \rangle$. The evaluation

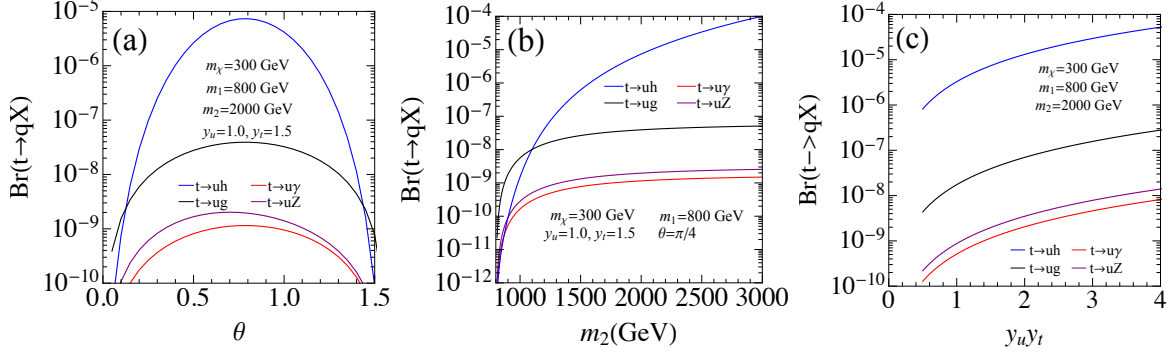


FIG. 2. The top quark FCNC decay branching ratios in our simplified model.

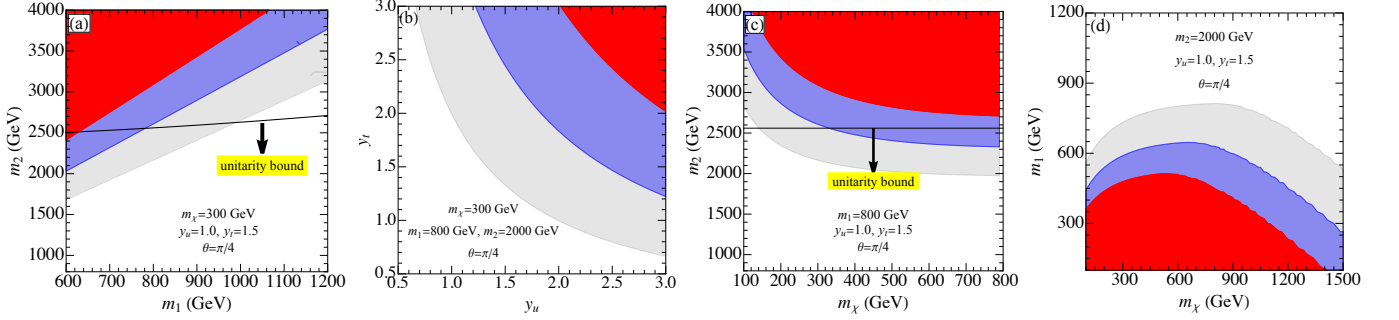


FIG. 3. The expected sensitivity to the model parameters through $t \rightarrow qh$ from the HL-LHC (red), HE-LHC (blue) and FCC-HH (gray) at 95% C.L.. The black line denotes the unitarity bound from the scattering $\phi_i \phi_j^* \rightarrow W_L^+ W_L^-$.

of DM density is controlled by the Boltzmann equation and its relic abundance is given by

$$\Omega_\chi h^2 \approx 2.76 \times 10^8 Y \frac{m_\chi}{\text{GeV}}, \quad (33)$$

where Y is the DM number density of today in the co-moving frame,

$$Y = \sqrt{\frac{45}{\pi}} \frac{g_*(x_f)^{1/2}/g_{*s}(x_f)}{m_{\text{PL}} m_\chi \langle \sigma v_{\text{rel}} \rangle} x_f. \quad (34)$$

Here $x_f \equiv m_\chi/T_f$, with T_f denoting the decoupling temperature and m_{PL} is the Planck mass. $g_*(x_f)$ and $g_{*s}(x_f)$ is the effective energy and entropy degree of freedom at the temperature of DM decoupling, respectively. Therefore, the minimal of the $\langle \sigma v_{\text{rel}} \rangle$ should be

$$\langle \sigma v_{\text{rel}} \rangle \approx 0.71 \frac{0.12}{\Omega_\chi h^2} \frac{x_f g_*(x_f)^{1/2}/g_{*s}(x_f)}{25 \cdot 0.1} \text{ pb}. \quad (35)$$

The annihilation cross section can be expanded based on the velocity, i.e. $\langle \sigma v_{\text{rel}} \rangle \doteq a + b \langle v_{\text{rel}}^2 \rangle + \mathcal{O}(\langle v_{\text{rel}}^4 \rangle)$. The coefficient a and b describes the contributions from s-wave and p-wave scattering, respectively. Since $\langle v_{\text{rel}}^2 \rangle \sim 0.3$ during the DM decoupling, the s-wave scattering will play the key role for the DM annihilation.

In the simplified model, the dominant contributions to DM annihilation come from s-wave processes $\chi\bar{\chi} \rightarrow t\bar{t}, t\bar{u}, u\bar{t}$ and p-wave processes $\chi\bar{\chi} \rightarrow u\bar{u}, d\bar{d}$; see Fig. 4. The s-wave contributions from $u\bar{u}$ and $d\bar{d}$ are suppressed by the quark mass due to the flip of the quark helicity and are ignored in the analysis. The annihilation cross sections are given as following,

$$\langle \sigma v_{\text{rel}} \rangle_{t\bar{t}} \simeq \frac{N_C y_t^4 m_t^2 (2m_\chi^2 + (m_2^2 - m_1^2) \cos(2\theta) + m_1^2 + m_2^2 - 2m_t^2)^2}{128\pi(m_\chi^2 + m_1^2 - m_t^2)^2(m_\chi^2 + m_2^2 - m_t^2)^2} \sqrt{1 - \frac{m_t^2}{m_\chi^2}}, \quad (36)$$

$$\langle \sigma v_{\text{rel}} \rangle_{t\bar{u}+u\bar{t}} \simeq \frac{N_C y_t^2 y_u^2 m_\chi^2 (m_1^2 - m_2^2)^2 \sin^2(2\theta)}{2\pi(2m_\chi^2 + 2m_1^2 - m_t^2)^2(2m_\chi^2 + 2m_2^2 - m_t^2)^2} \left(1 - \frac{m_t^2}{4m_\chi^2}\right)^2, \quad (37)$$

$$\begin{aligned} \langle \sigma v_{\text{rel}} \rangle_{u\bar{u}} \simeq & \frac{y_u^4}{64\pi(m_\chi^2 + m_1^2)^4(m_\chi^2 + m_2^2)^4} \{m_\chi^2 m_1^4 m_2^4 \Delta^2 + 8m_\chi^4 m_1^4 m_2^4 \Delta \\ & + m_\chi^6 [(m_1^4 + m_2^4) \Delta^2 + 20m_1^4 m_2^4] + 4m_\chi^8 [(m_1^2 + m_2^2) \Delta^2 + 4m_1^2 m_2^2 (m_2^2 - m_1^2) \cos(2\theta)] \\ & + m_\chi^{10} [5\Delta^2 + 4(m_1^4 + m_2^4)] + 8m_\chi^{12} \Delta + 4m_\chi^{14}\} v_{\text{rel}}^2, \end{aligned} \quad (38)$$

$$\langle \sigma v_{\text{rel}} \rangle_{d\bar{d}} \simeq \frac{y_u^4 m_\chi^2 (m_\chi^2 + M_2^2)}{16\pi(m_\chi^2 + M_2^2)^4} v_{\text{rel}}^2, \quad (39)$$

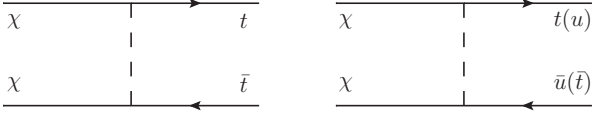


FIG. 4. Majorana dark matter annihilation processes.

where $N_C = 3$ denotes the color factor of quarks and $\Delta = m_1^2 + m_2^2 - (m_2^2 - m_1^2) \cos(2\theta)$. As we expected that the annihilation from $t\bar{t}$ mode contributes to the s-wave and the rate is proportional to m_t due to the flip of the quark helicity, while $u\bar{u}$ and $d\bar{d}$ modes will only contribute to the p-wave when we ignore their mass. Furthermore, the annihilation to $t\bar{u}$ and $u\bar{t}$ final states come from the mixing of the scalars Φ_1 and Φ_2 , thus the rates are proportional to the mixing angle $\sin(2\theta)$.

In Fig. 5(a), we show the relic density in our simplified model with the benchmark parameters $m_\chi = 300$ GeV, $m_1 = 800$ GeV, $y_u = 1$, $y_t = 1.5$ and $\theta = \pi/4$. The black line represents the upper limit from Planck 2018 at 2σ level [65]. We note that the relic density approaches a constant in the large m_2 region due to the decoupling behavior of ϕ_2 . Its effects could be understood from the thermal cross sections $\langle \sigma v_{\text{rel}} \rangle_{t\bar{u}+u\bar{t}}$ and $\langle \sigma v_{\text{rel}} \rangle_{t\bar{t}}$ in the limit of $m_2 \rightarrow \infty$:

$$\langle \sigma v_{\text{rel}} \rangle_{t\bar{t}} \simeq \frac{N_C y_t^4 m_t^2 (1 + \cos(2\theta))^2}{128\pi(m_1 + m_\chi - m_t)^2} \sqrt{1 - m_t^2/m_\chi^2}, \quad (40)$$

$$\langle \sigma v_{\text{rel}} \rangle_{t\bar{u}+u\bar{t}} \simeq \frac{N_C y_t^2 y_u^2 m_\chi^2 \sin^2(2\theta)}{8\pi(2m_1^2 + 2m_\chi^2 - m_t^2)^2} \sqrt{1 - m_t^2/4m_\chi^2}. \quad (41)$$

We show the allowed parameter space on the plane (m_1, m_2) and (m_χ, m_1) from Planck 2018 at 2σ level [65] in Fig. 5(b) and Fig. 5(c), respectively. It shows that the parameter space will be constrained seriously by the DM relic density measurement in the decoupling limit of $m_{1,2} \gg m_\chi$.

B. direct detection

Direct detection is one of cornerstones of DM searches. The goal of direct detection experiments is to detect the rare scattering between the non-relativistic DM and the target material; see Fig. 6. The scattering cross sections could be separated into spin-independent (SI) and spin-dependent (SD) contributions based on the interactions between DM and the nucleus. Since the SI scattering resolves the entire nucleus coherently, the cross section will be enhanced by the squared number of scattering centers (nucleons). While for the SD scattering, DM couples to the nucleon spin and the coherent enhancement effect disappears. To describe the SI and SD scatterings, we use the following effective Lagrangian [66, 67],

$$\mathcal{L} = \sum_{u,d} f_q^{\text{SD}} \bar{\chi} \gamma^\mu \gamma^5 \chi \bar{q} \gamma_\mu \gamma^5 q + \sum_{u,d,s} \mathcal{L}_q^{\text{EFT}} + \mathcal{L}_g^{\text{EFT}}, \quad (42)$$

where

$$\begin{aligned} \mathcal{L}_q^{\text{EFT}} = & f_q m_q \bar{\chi} \chi \bar{q} q + \frac{g_q^{(1)}}{2m_\chi} \bar{\chi} i(\partial^\mu \gamma^\nu + \partial^\nu \gamma^\mu) \chi O_{q,\mu\nu}^{(2)} \\ & + \frac{g_q^{(2)}}{m_\chi^2} \bar{\chi} (i\partial^\mu) (i\partial^\nu) \chi O_{q,\mu\nu}^{(2)}, \end{aligned} \quad (43)$$

$$\begin{aligned} \mathcal{L}_g^{\text{EFT}} = & f_G \bar{\chi} \chi G_{\mu\nu}^a G^{a\mu\nu} + \frac{g_G^{(1)}}{2m_\chi} \bar{\chi} i(\partial^\mu \gamma^\nu + \partial^\nu \gamma^\mu) \chi O_{G,\mu\nu}^{(2)} \\ & + \frac{g_G^{(2)}}{m_\chi^2} \bar{\chi} (i\partial^\mu) (i\partial^\nu) \chi O_{G,\mu\nu}^{(2)}. \end{aligned} \quad (44)$$

The twist-2 operators $O_{q,\mu\nu}^{(2)}$ and $O_{G,\mu\nu}^{(2)}$ are defined as

$$O_{q,\mu\nu}^{(2)} \equiv \frac{1}{2} \bar{q} (\gamma^{\{\mu} i D_-^{\nu\}} - \frac{g^{\mu\nu}}{4} i \not{D}) q, \quad (45)$$

$$O_{G,\mu\nu}^{(2)} \equiv -G^{a\mu\lambda} G_{\lambda}^{a\nu} + \frac{g^{\mu\nu}}{4} (G^a_{\alpha\beta})^2. \quad (46)$$

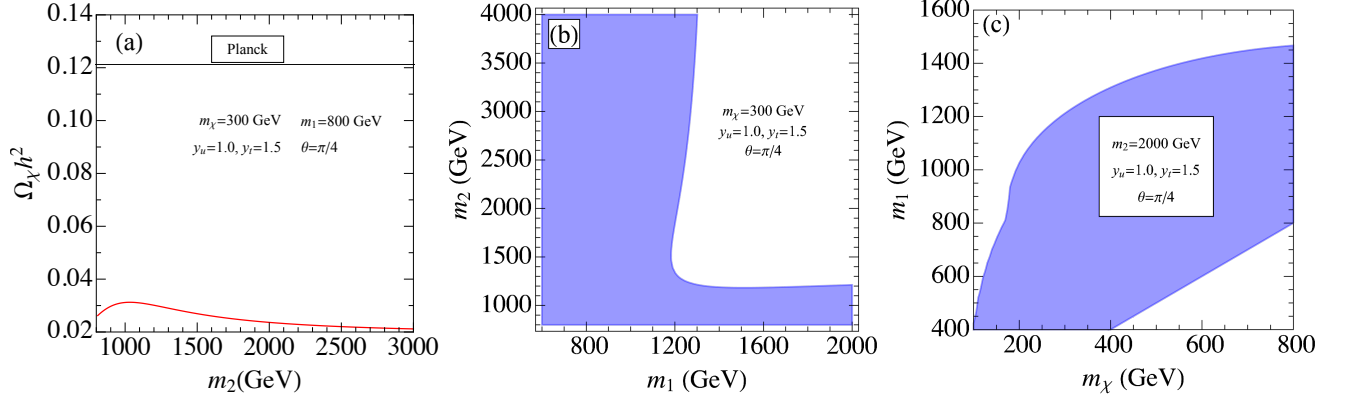


FIG. 5. Dark matter relic abundance and limits from Planck 2018 [65]

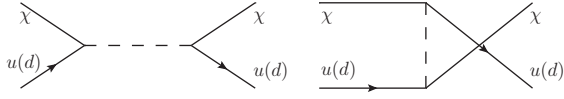


FIG. 6. DM direct detection process at the tree level.

Here

$$\gamma^{\{\mu} i D_-^{\nu\}} = \frac{1}{2} i (\gamma^\mu D_-^\nu + D_-^\mu \gamma^\nu), \quad D_-^\mu = D^\mu - \not{D}^\mu. \quad (47)$$

The Wilson coefficients f_q^{SD} , f_j and $g_j^{(i)}$ with $j = q, G$ and $i = 1, 2$ could match to our simplified model. It is clear that f_q^{SD} term describes the SD scattering, while $\mathcal{L}_q^{\text{EFT}}$ and $\mathcal{L}_G^{\text{EFT}}$ contribute to the SI process. The matrix element of DM SD scattering with a nucleon target ($N = p$ or n) is

$$f^{\text{SD}} = \sum_{u,d} f_q^{\text{SD}} \Delta_N^q. \quad (48)$$

The hadronic matrix element Δ_N^q is defined through

$$\langle N | \bar{q} \gamma^\mu \gamma^5 q | N \rangle = 2s^\mu \Delta_N^q, \quad (49)$$

where s^μ is the spin of the nucleon. Meanwhile, the matrix element of the SI scattering is

$$\begin{aligned} f_N/m_N = & \sum_{u,d,s} f_{Tq} f_q + \sum_{u,d,s,c,b} \frac{3}{4} [q(2) + \bar{q}(2)] (g_q^{(1)} + g_q^{(2)}) \\ & - \frac{8\pi}{9\alpha_s} f_{TG} f_G + \frac{3}{4} G(2) (g_G^{(1)} + g_G^{(2)}), \end{aligned} \quad (50)$$

where m_N is the nucleon mass and f_{Tq} , f_{TG} , $q(2)$, $\bar{q}(2)$ and $G(2)$ are hadronic matrix elements:

$$\langle N | m_q \bar{q} q | N \rangle = f_{Tq} m_N, \quad (51)$$

$$\langle N | G_{\mu\nu}^a G^{a\mu\nu} | N \rangle = -\frac{8\pi}{9\alpha_s} f_{TG} m_N, \quad (52)$$

$$\langle N | O_{q,\mu\nu}^{(2)} | N \rangle = \frac{1}{m_N} (p_\mu p_\nu - \frac{1}{4} m_N^2 g_{\mu\nu}) (q(2) + \bar{q}(2)), \quad (53)$$

$$\langle N | O_{G,\mu\nu}^{(2)} | N \rangle = \frac{1}{m_N} (p_\mu p_\nu - \frac{1}{4} m_N^2 g_{\mu\nu}) G(2). \quad (54)$$

Here p is the momentum of the nucleon.

With these conventions, the SD and SI cross sections can be written as

$$\sigma_{\chi N}^{\text{SD}} = \frac{12\mu_N^2}{\pi} (f^{\text{SD}})^2, \quad \sigma_{\chi N}^{\text{SI}} = \frac{4\mu_N^2}{\pi} f_N^2, \quad (55)$$

where μ_N is the reduced mass of the nucleon and DM, i.e. $\mu_N = m_N m_\chi / (m_N + m_\chi)$. The SD scattering is dominated by the tree level interactions and the matching coefficient f_q^{SD} could be got at the leading order with the large mass expansion of the mediators $\phi_{1,2,d}$. The detail of the calculation could be found in Refs. [53, 55] and the results are

$$f_u^{\text{SD}} = -\frac{y_u^2}{8} \left[\frac{\sin^2 \theta}{m_\chi^2 - m_1^2} + \frac{\cos^2 \theta}{m_\chi^2 - m_2^2} \right], \quad (56)$$

$$f_d^{\text{SD}} = -\frac{y_u^2}{8} \frac{1}{m_\chi^2 - M_2^2}. \quad (57)$$

While the leading order cross section for the SI scattering will vanish due to the Majorana nature of the DM, as a result, it is necessary to go beyond the leading order in order to estimate the rate of SI scattering. The matching coefficients f_q and $g_q^{(1)}$ could be got from the next-to-leading order expansion of the mediator $\phi_{1,2,d}$ propaga-

tors, i.e.

$$f_u = \frac{y_u^2 \sin^2 \theta}{16} \frac{m_\chi}{(m_\chi^2 - m_1^2)^2} + \frac{y_u^2 \cos^2 \theta}{16} \frac{m_\chi}{(m_\chi^2 - m_2^2)^2}, \quad (58)$$

$$f_d = \frac{y_u^2}{16} \frac{m_\chi}{(m_\chi^2 - M_2^2)^2}, \quad (59)$$

$$g_u^{(1)} = \frac{y_u^2 \sin^2 \theta}{4} \frac{m_\chi}{(m_\chi^2 - m_1^2)^2} + \frac{y_u^2 \cos^2 \theta}{4} \frac{m_\chi}{(m_\chi^2 - m_2^2)^2}, \quad (60)$$

$$g_d^{(1)} = \frac{y_u^2}{4} \frac{m_\chi}{(m_\chi^2 - M_2^2)^2}. \quad (61)$$

It shows that the SI matching coefficients f_q and $g_q^{(1)}$ are suppressed by factor $1/(m^2 - m_\chi^2)$, with $m = m_{1,2}, M_2$

compared to the f_q^{SD} in the region of we are interested in, i.e. $m_\chi \ll m_{1,2}, M_2$.

The SI matching coefficients f_G and $g_G^{(1,2)}$ could be induced at the one loop and can be calculated by the usual Feynman diagrams with the help of the projection operators. Alternatively, one can also use the Fock-Schwinger gauge to simplify the calculation [55, 66, 68], i.e. $x^\mu A_\mu = 0$. In this work, we will focus on the Fock-Schwinger gauge method and refer the reader to Ref. [55] for the detail of projection operator approach. In the Fock-Schwinger gauge, one can express the gluon field in terms of its field strength tensor $G_{\mu\nu}$ and maintain explicit gauge invariance for each step in the calculation. The Wilson coefficients can be extracted from the one loop correction to a Majorana fermion propagator through a non-zero background of gluon fields and it shows

$$\begin{aligned} f_G = \frac{\alpha_s}{32\pi} \Big\{ & y_t^2 m_t^2 \left[\int \frac{d^4 q}{i\pi^2} \frac{(\not{p} + \not{q}) \cos^2 \theta}{(q^2 - m_1^2)[(p+q)^2 - m_t^2]^4} + \int \frac{d^4 q}{i\pi^2} \frac{(\not{p} + \not{q}) \sin^2 \theta}{(q^2 - m_2^2)[(p+q)^2 - m_t^2]^4} \right] \\ & + y_t^2 m_1^2 \int \frac{d^4 q}{i\pi^2} \frac{(\not{p} + \not{q}) \cos^2 \theta}{[(q^2 - m_1^2)^4][(p+q)^2 - m_t^2]} + y_t^2 m_2^2 \int \frac{d^4 q}{i\pi^2} \frac{(\not{p} + \not{q}) \sin^2 \theta}{[(q^2 - m_2^2)^4][(p+q)^2 - m_t^2]} \\ & + y_u^2 m_1^2 \int \frac{d^4 q}{i\pi^2} \frac{(\not{p} + \not{q}) \sin^2 \theta}{[(q^2 - m_1^2)^4](p+q)^2} + y_u^2 m_2^2 \int \frac{d^4 q}{i\pi^2} \frac{(\not{p} + \not{q}) \cos^2 \theta}{[(q^2 - m_2^2)^4](p+q)^2} + y_u^2 M_2^2 \int \frac{d^4 q}{i\pi^2} \frac{\not{p} + \not{q}}{[(q^2 - M_2^2)^4](p+q)^2} \Big\}. \end{aligned} \quad (62)$$

The loop integration in Eq. 62 can be calculated analytically and we show the detail in the Appendix.

The Wilson coefficients of gluon twist-2 operators could be obtained from the scattering matrix element,

$$\begin{aligned} M_{\text{twist-2}} = 2\pi\alpha_s \bar{\chi} [& f(y_t \cos \theta, m_t, m_1) + f(y_t \sin \theta, m_t, m_2) \\ & + f(y_u \sin \theta, 0, m_1) + f(y_u \cos \theta, 0, m_2) + f(y_u, 0, M_2)] \chi O_{G,\mu\nu}^{(2)} \end{aligned} \quad (63)$$

where the function $f(g_\chi, m_q, m_\phi)$ is defined as

$$\begin{aligned} f(g_\chi, m_q, m_\phi) = g_\chi^2 \int \frac{d^4 q}{(2\pi)^2} \frac{\gamma^\mu (p+q)^\nu + \gamma^\nu (p+q)^\mu}{(q^2 - m_\phi^2)[(p+q)^2 - m_q^2]^3} \\ + g_\chi^2 \int \frac{d^4 q}{(2\pi)^2} \frac{(\not{p} + \not{q})[-m_q^2 g^{\mu\nu} - 2(p+q)^\mu (p+q)^\nu]}{(q^2 - m_\phi^2)[(p+q)^2 - m_q^2]^4} \\ + \frac{1}{2} g_\chi^2 \int \frac{d^4 q}{(2\pi)^2} \frac{(\not{p} + \not{q})[(q^2 - m_\phi^2)g^{\mu\nu} - 4q^\mu q^\nu]}{(q^2 - m_\phi^2)^4[(p+q)^2 - m_q^2]}. \end{aligned} \quad (64)$$

Therefore, the twist-2 Wilson coefficients are

$$\begin{aligned} g_G^{(1)} = -\frac{\alpha_s}{96\pi m_\chi^3 \Delta} \Big[& g_1(y_t \cos \theta, m_t, m_1) + g_1(y_t \sin \theta, m_t, m_2) \\ & + g_1(y_u \sin \theta, 0, m_1) + g_1(y_u \cos \theta, 0, m_2) + g_1(y_u, 0, M_2) \Big], \end{aligned} \quad (65)$$

$$\begin{aligned} g_G^{(2)} = \frac{\alpha_s}{48\pi m_\chi^3 \Delta^2} \Big[& g_2(y_t \cos \theta, m_t, m_1) + g_2(y_t \sin \theta, m_t, m_2) \\ & + g_2(y_u \sin \theta, 0, m_1) + g_2(y_u \cos \theta, 0, m_2) + g_2(y_u, 0, M_2) \Big], \end{aligned} \quad (66)$$

where

$$g_1(g_\chi, m_q, m_\phi) = g_\chi^2 \left\{ [5m_\chi^4 m_q^2 + m_\chi^4 m_\phi^2 - 3m_\chi^2 m_q^4 + 3m_\chi^2 m_\phi^4 + (m_q^2 - m_\phi^2)^3 - 3m_\chi^6] L - 6m_\chi^4 + 2m_\chi^2 (m_q^2 - m_\phi^2) + \Delta \ln \frac{m_q^2}{m_\phi^2} \right\}, \quad (67)$$

$$g_2(g_\chi, m_q, m_\phi) = g_\chi^2 \left\{ [m_\chi^8 (m_q^2 - 5m_\phi^2) + 2m_\chi^6 (2m_q^2 m_\phi^2 - 4m_q^4 + 5m_\phi^4) + 10m_\chi^4 (m_q^6 - m_\phi^6) - 5m_\chi^2 (m_q^2 - m_\phi^2)^3 (m_q^2 + m_\phi^2) + (m_q^2 - m_\phi^2)^5 + m_\chi^{10}] L + 2m_\chi^6 (m_q^2 - 4m_\phi^2) 7m_\chi^4 (m_\phi^4 - m_q^4) + 2m_\chi^2 (m_q^2 - m_\phi^2)^3 + 3m_\chi^8 + \Delta^2 \ln \frac{m_\phi^2}{m_q^2} \right\}. \quad (68)$$

The definition of Δ and L could be found in the Appendix; see Eqs. A5 and A6.

Next, we perform a numerical calculation for $\sigma_{\chi N}^{\text{SD}}$ and $\sigma_{\chi N}^{\text{SI}}$. The hadronic matrix elements are given by [69]:

$$\begin{aligned} f_{Tu}^p &= 0.018, & f_{Td}^p &= 0.030, & f_{Tu}^n &= 0.015, \\ f_{Td}^n &= 0.034, & f_{TG} &= 0.80. \end{aligned} \quad (69)$$

Here f_{Tq}^N corresponds to the contribution of the quark q to the nucleon matrix elements for the nucleon N . The matrix elements of the twist-2 operators are related to the second moments of the parton distribution functions (PDFs),

$$q(2) + \bar{q}(2) = \int_0^1 dx x (q(x) + \bar{q}(x)), \quad G(2) = \int_0^1 dx x g(x), \quad (70)$$

where $q(x)$, $\bar{q}(x)$ and $g(x)$ are the PDFs of quark, anti-quark and gluon in nucleon N , respectively. Those hadronic elements could be extracted from the CT14NNLO PDFs [70],

$$\begin{aligned} [u(2) + \bar{u}(2)]_p &= 0.3481, & [d(2) + \bar{d}(2)]_p &= 0.1902, \\ G(2)_p &= G(2)_n = 0.4159. \end{aligned} \quad (71)$$

For the spin dependent matrix elements, we utilize the values in Ref. [71],

$$\Delta_p^u = 0.84, \quad \Delta_p^d = -0.43, \quad \Delta_n^u = -0.43, \quad \Delta_n^d = 0.84. \quad (72)$$

We show the DM SD and SI scattering rates in Figs. 7(a)-(c) (red lines), with the benchmark parameters $m_\chi = 300$ GeV, $m_1 = 800$ GeV, $y_u = 1$, $y_t = 1.5$ and $\theta = \pi/4$. The most severe limits for the SD scattering with proton and neutron targets are from PICO-60 [72] and XENON1T [73], respectively, and the upper limits are roughly $\mathcal{O}(10^{-40} \text{cm}^2)$ (black meshed regions). The SI scattering measurement from XENON1T could give a stronger bound for the cross section [73] (black meshed region), i.e. $\sigma_{\chi p}^{\text{SI}} \sim 10^{-45} \text{cm}^2$. While the expected constraints from XENON20T [46] (blue regions) and DARWIN [47] (purple region) could be further improved as

compared to the present data and it shows the sensitivity could be enhanced about one to two order of magnitude for both the SD and SI scattering. We observe that the predictions from our simplified model are consistent with the current measurements and also could be tested in the future experiments. In addition, we note that the cancellation between up and down quarks' contributions in DM-neutron SD scattering will obviously change the cross section compared to the DM-proton SD process; see Fig. 7(b) (red lines). In Figs. 7(d)-(f), we show the expected sensitivity regions from the future XENON20T and DARWIN experiments on the plane of m_1 and m_2 . It is clear that both the DM-neutron SD and SI scattering could give a strong constraint for our simplified model and the measurements could probe complementary regions in the parameter space.

V. COLLIDER SEARCH AT THE LHC

In this section we dedicate to explore the LHC limits to our simplified model. The processes of interests to us at the LHC include pair production of the colored scalars (ϕ_i , with $i = 1, 2, d$) and the associated production of scalars with DM candidate χ . It has been shown that the later process plays a subdominant role to constrain the model parameter space, and will be neglected from here on [55]. The pair production of scalars could be generated through the strong force and the Yukawa interactions; see Fig. 8. We should note that those colored scalars have the same performance as the squarks in the supersymmetric models at the LHC, as a result, we can use the limits from squark searches at the LHC to estimate the bounds of our simplified model [74].

The colored scalar $\phi_{1,2,d}$ could decay to light quark/top quark plus DM candidate χ and both of them have been searched by ATLAS and CMS collaborations [74–77]. It shows that the bounds from the top quark decay mode are much weaker than the light quark case in the most parameter space [74]. Therefore, we will only consider the light quark decay mode in this work, i.e. $\phi_{1,2} \rightarrow u\chi$ and $\phi_d \rightarrow d\chi$.

We generate the parton level events at 13 TeV LHC using MadGraph5 [78] and pass them to PYTHIA [79]

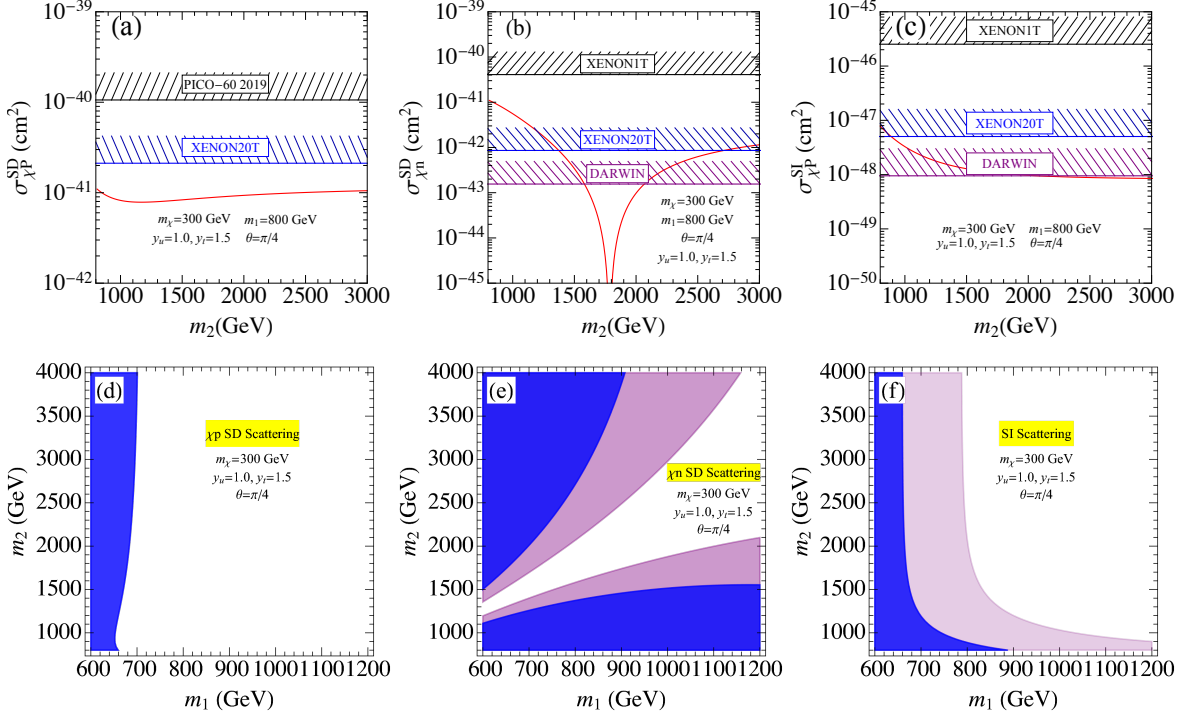


FIG. 7. The constraints from DM direct detection experiments on the parameter m_2 (a,b,c) and m_1 - m_2 plane (d,e,f). The black meshed region denotes the limits from the current measurements PICO-60 and XENON1T, while the blue and purple meshed (shaded) regions are the bound from the future XENON20T and DARWIN, respectively.

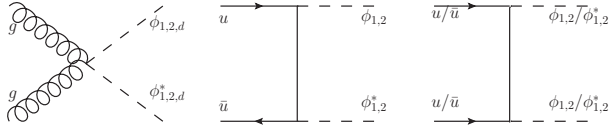


FIG. 8. Illustrative Feynman diagrams of colored scalar pair production at the LHC.

for showering and hadroniation, and simulate the collider smearing effects utilizing Delphes [80]. Then, following the analysis strategy of CMS collaboration [74], we require the following kinematic cuts on the events:

$$\begin{aligned} n_j &= 2-3, \quad n_b = 0, \quad |\eta^j| < 2.4, \quad p_T^j > 30 \text{ GeV}, \\ H_T &> p_T^{\text{miss}} > 300 \text{ GeV}, \quad \Delta\phi(\vec{p}_T^{\text{miss}}, j_1) > 0.5, \\ \Delta\phi(\vec{p}_T^{\text{miss}}, j_2) &> 0.5, \quad \Delta\phi(\vec{p}_T^{\text{miss}}, j_3) > 0.3, \end{aligned} \quad (73)$$

where $n_{j(b)}$ is the light (bottom) jet number, H_T is the scalar p_T sum of jets with $|\eta^j| < 2.4$ and p_T^{miss} is the missing transverse momentum. The CMS search is performed in a four-dimensional region defined by exclusive intervals in n_j , n_b , H_T and p_T^{miss} . Based on the signal features of our model, we fix n_j and n_b in the analysis, while including the 10 kinematic intervals of H_T and p_T^{miss} which are defined in Ref. [74]. The significance for each bin q_{EL} could be evaluated by the likelihood method and

it shows

$$q_{\text{EL}} = \sqrt{-2 \left[N_{\text{Exp}} \ln \frac{N_s + N_b}{N_b} - N_s \right]}, \quad (74)$$

where N_{Exp} , N_s and N_b denote the number of observed, signal and SM background events, respectively. The N_{Exp} and N_b for each bin can be found in Ref. [74] and the systematic uncertainties for the background will be ignored in this analysis. The total significance for the 10 bins could be obtained by square root sum of each bin.

Figure 9(a) shows the allowed parameter space on the plane of m_χ and m_1 with benchmark parameters $m_2 = 2000 \text{ GeV}$, $y_u = 1.0$, $y_t = 1.5$ and $\theta = \pi/4$ at the 95% C.L. with the integrated luminosity of 137 fb^{-1} based on above analysis. It shows that the same-sign electric charged scalar pair production through Yukawa interaction could play a crucial role in some parameter space due to the enhancement of the up quark PDF [81]. We displays the combined constraints from the DM searches at the LHC (blue meshed region), $t \rightarrow qh$ measurement from FCC-hh (gray region) and projected DM SD (purple region) and SI (red region) scattering from DARWIN on the plane of m_1 and m_2 at 2σ level in Fig. 9(b). The meshed region was excluded by the 13 TeV LHC data, while the colored regions could be probed by the future experiments. It is clearly that the direct detection experiments, DM LHC searches and top quark FCNC measurement could probe complementary and same regions in parameter space.

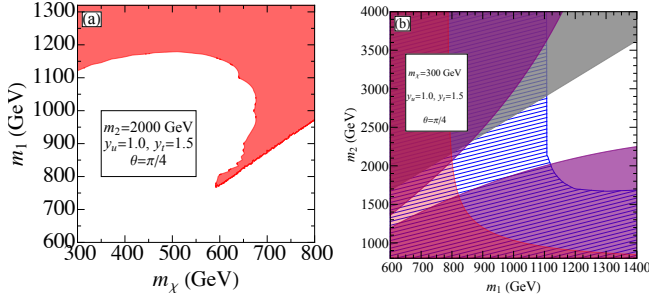


FIG. 9. (a) Allowed parameter space under the constraint from the 13 TeV LHC with an integrated luminosity of 137 fb^{-1} at 2σ level on the plane of m_χ and m_1 . (b) Combined constraints to the parameter space on the plane of m_1 and m_2 . The blue meshed region was excluded by the 13 TeV LHC at 2σ level with an integrated luminosity of 137 fb^{-1} . The colored region can be probed from tqh search at the FCC-hh (gray region), spin-dependent (purple region) and spin-independent (red region) DM direct detection search at the projected DARWIN experiment, respectively.

Before closing this section, we would like to scan the 5-dim parameter space $\{m_{1,2,\chi}, y_u, y_t\}$ to estimate the allowed parameter space within all constraints and the results are shown in Fig. 10. In order to enhance the top quark FCNC effects, we choose the maximal mixing angle of $\theta = \pi/4$ in this study. We consider the following parameter space with assumption $m_\chi < m_{1,2,d}$,

$$\begin{aligned} y_u &\in [0.4, 2.0], & y_t &\in [0.4, 2.0], \\ m_1 &\in [800, 2000] \text{ GeV}, & m_2 &\in [1000, 4000] \text{ GeV}, \\ m_\chi &\in [300, 1200] \text{ GeV}. \end{aligned}$$

We project the points from 5-dim space to the plane of (m_1, m_2) and (m_χ, m_1) . All points denote the parameters which are consistent with the current LHC limit and dark matter relic abundance measurement from Planck at 2σ level. The red points describe the parameters which can be tested via $t \rightarrow qh$ at the future collider FCC-HH and the blue points imply the parameters can be crosschecked via the tqh search and DM direct detection experiments from DARWIN, including both the spin-independent and spin-dependent scatterings. The black line in the plane (m_1, m_2) denotes the unitarity bound. It shows that both the top quark FCNC signal and DM direct detection experiments play an important role to constrain the parameter space of our simplified model.

VI. CONCLUSION

Due to the large hierarchy between the top quark FCNC anomalous couplings and the SM top quark interactions, it is well motivated to study the loop induced top quark FCNC processes at the LHC, which could avoid the possible unduly small NP couplings in the model. In this work, we consider one class of the simplified model

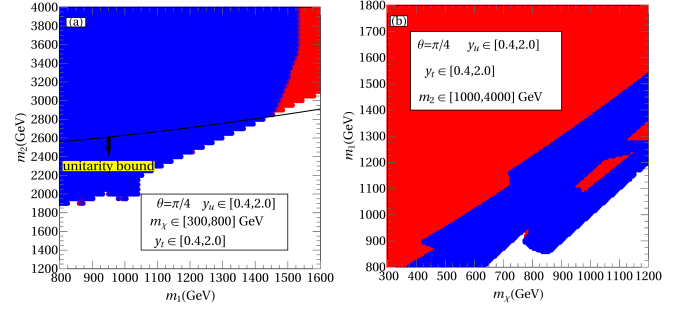


FIG. 10. Parameters scanning in the 5-dim parameter space $\{m_1, m_2, m_\chi, y_u, y_t\}$. To maximize the top quark FCNC effects, we choose the maximal mixing angle of $\theta = \pi/4$. The points in the figures denote the parameters which are consistent with the current LHC DM limit and DM relic abundance measurement from Planck at 2σ level. The red points can be probed via top quark FCNC coupling tqh measurement at the FCC-HH, while the blue points can be probed by both the tqh at the FCC-HH and DM direct detection experiment DARWIN (both spin-dependent and spin independent).

which could only generate the top quark FCNC couplings in the loop level. Such scenario predicts a Majorana dark matter candidate and could be tested through the scattering between the dark matter and the nuclei, and also the data from LHC.

In our simplified model, the top quark could decay to $q + Z/\gamma/g/h$ and the most promising decay channel at the HL-LHC and future hadron colliders would be $t \rightarrow qh$. Its branching ratio is around $\mathcal{O}(10^{-5})$ in some parameter space. Comparing to the expected limits from the HL-LHC, the unitarity band from $\phi\phi \rightarrow W_L W_L$ scattering would give a stronger constraint for the model parameters.

To fully explore the discovery potential of our simplified model, we carried out a comprehensive comparison of the dark matter relic density, direct detection experiments and LHC searches. Due to the Majorana nature of the dark matter in our model, we note that the SI scattering with nuclei at leading order will vanish, while it could be generated at the next-to-leading order. Although the SI cross section from higher order will be suppressed compared to the tree level SD case, the SI scattering also provides a comparable limits to the SD production. Our analysis shows that the simplified model could easily satisfy the relic density limits, while the direct detection experiments from the scattering between dark matter and nuclei and LHC searches provide the severe bounds. In particular, the constraints from scattering between dark matter and neutron. When comparing the direct detection experiments and LHC searches, we note that they could probe complementary and same regions in parameter space, and are both necessary to fully constrain our simplified model.

ACKNOWLEDGMENTS

We thank Qing-Hong Cao, Zhaofeng Kang, Jue Zhang and Ya Zhang for helpful discussions. The work of Y. Liu is supported in part by the National Science Foundation of China under Grant Nos. 11805013, 12075257 and the Fundamental Research Funds for the Central Universities under Grant No. 2018NTST09, BY is supported by the U.S. Department of Energy, Office of Science, Office of Nuclear Physics, under Contract DE-AC52-06NA25396, [under an Early Career Research Award (C. Lee),] and through the LANL/LDRD Program, RZ is supported in part by the National Science Foundation of China under Grant Nos. 12075257 and the funding from the Institute of High Energy Physics, Chinese Academy of Sciences (Y6515580U1) and the funding from Chinese Academy of Sciences (Y8291120K2).

Appendix A: Feynman Integral

In the appendix we represent the details of the Feynman integrals in Eq. 62,

$$\int \frac{d^4 q}{i\pi^2} \frac{(\not{p} + \not{q})}{(q^2 - m_\phi^2)[(p+q)^2 - m_q^2]^4}, \quad (\text{A1})$$

and

$$\int \frac{d^4 q}{i\pi^2} \frac{(\not{p} + \not{q})}{(q^2 - m_\phi^2)^4[(p+q)^2 - m_q^2]}. \quad (\text{A2})$$

Note we can substitute \not{p} with m_χ in terms of Dirac equation of dark matter field with momentum p . Utilizing the Feynman parametrization method, we obtain

$$\begin{aligned} & \int \frac{d^4 q}{i\pi^2} \frac{(\not{p} + \not{q})}{(q^2 - m_\phi^2)[(p+q)^2 - m_q^2]^4} \\ &= \frac{6m_q^2 m_\phi^2 (m_\phi^2 + m_q^2 - m_\chi^2)L + \Delta - 12m_q^2 m_\phi^2}{6m_q^4 \Delta^2}, \end{aligned} \quad (\text{A3})$$

and

$$\begin{aligned} & \int \frac{d^4 q}{i\pi^2} \frac{(\not{p} + \not{q})}{(q^2 - m_\phi^2)^4[(p+q)^2 - m_q^2]} \\ &= \frac{(\Delta + 6m_\phi^2 m_q^2)(m_\phi^2 + m_q^2 - m_\chi^2) - 12m_q^4 m_\phi^4 L}{6m_\phi^4 \Delta^2}, \end{aligned} \quad (\text{A4})$$

where the symbols Δ and L are defined as

$$\Delta = 4m_\phi^2 m_\chi^2 - (m_q^2 - m_\chi^2 - m_\phi^2)^2, \quad (\text{A5})$$

and

$$L = \begin{cases} \frac{2}{\sqrt{|\Delta|}} \tanh^{-1} \frac{\sqrt{|\Delta|}}{m_q^2 + m_\phi^2 - m_\chi^2}, & \Delta < 0 \\ \frac{4m_\chi^2}{m_q^4 + m_\phi^4 - m_\chi^4 - 2m_q^2 m_\phi^2}, & \Delta = 0 \\ \frac{2}{\sqrt{\Delta}} \tanh^{-1} \frac{\sqrt{\Delta}}{m_q^2 + m_\phi^2 - m_\chi^2}. & \Delta > 0 \end{cases} \quad (\text{A6})$$

-
- [1] S. L. Glashow, J. Iliopoulos, and L. Maiani, Phys. Rev. **D2**, 1285 (1970).
 - [2] J. Aguilar-Saavedra, Acta Phys. Polon. B **35**, 2695 (2004), hep-ph/0409342.
 - [3] R. Gaitán, J. H. Montes de Oca, E. A. Garcés, and R. Martínez, Phys. Rev. **D94**, 094038 (2016), 1503.04391.
 - [4] G. Abbas, A. Celis, X.-Q. Li, J. Lu, and A. Pich, JHEP **06**, 005 (2015), 1503.06423.
 - [5] A. Arhrib, R. Benbrik, C.-H. Chen, M. Gomez-Bock, and S. Semlali, Eur. Phys. J. **C76**, 328 (2016), 1508.06490.
 - [6] K. Y. Oyulmaz, A. Senol, H. Denizli, A. Yilmaz, I. Turk Cakir, and O. Cakir, Eur. Phys. J. C **79**, 83 (2019), 1811.01074.
 - [7] L. Shi and C. Zhang, Chin. Phys. C **43**, 113104 (2019), 1906.04573.
 - [8] H. Khanpour, Nucl. Phys. B **958**, 115141 (2020), 1909.03998.
 - [9] J.-j. Cao, G.-l. Liu, J. M. Yang, and H.-j. Zhang, Phys. Rev. **D76**, 014004 (2007), hep-ph/0703308.
 - [10] J. M. Yang, Int. J. Mod. Phys. **A23**, 3343 (2008), 0801.0210.
 - [11] J. J. Zhang, C. S. Li, J. Gao, H. Zhang, Z. Li, C. P. Yuan, and T.-C. Yuan, Phys. Rev. Lett. **102**, 072001 (2009), 0810.3889.
 - [12] X.-F. Han, L. Wang, and J. M. Yang, Phys. Rev. **D80**, 015018 (2009), 0903.5491.
 - [13] C.-X. Yue, J. Wang, Y. Yu, and T.-T. Zhang, Phys. Lett. **B705**, 222 (2011), 1105.5227.
 - [14] J. Gao, C. S. Li, L. L. Yang, and H. Zhang, Phys. Rev. Lett. **107**, 092002 (2011), 1104.4945.
 - [15] J. Cao, C. Han, L. Wu, J. M. Yang, and M. Zhang, Eur. Phys. J. **C74**, 3058 (2014), 1404.1241.
 - [16] H. Sun, Nucl. Phys. **B886**, 691 (2014), 1402.1817.
 - [17] W. Liu, H. Sun, X. Wang, and X. Luo, Phys. Rev. **D92**, 074015 (2015), 1507.03264.
 - [18] H. Sun and X. Wang, Eur. Phys. J. **C78**, 281 (2018), 1602.04670.
 - [19] X. Wang, H. Sun, and X. Luo, Adv. High Energy Phys. **2017**, 4693213 (2017), 1703.02691.
 - [20] V. Khachatryan et al. (CMS), JHEP **04**, 035 (2016), 1511.03951.
 - [21] G. Aad et al. (ATLAS), Phys. Lett. B **800**, 135082 (2020), 1908.08461.
 - [22] F. Abe et al. (CDF), Phys. Rev. Lett. **80**, 2525 (1998).
 - [23] V. Khachatryan et al. (CMS), JHEP **02**, 028 (2017), 1610.03545.
 - [24] G. Aad et al. (ATLAS), Eur. Phys. J. **C76**, 55 (2016), 1509.00294.
 - [25] T. Aaltonen et al. (CDF), Phys. Rev. Lett. **102**, 151801 (2009), 0812.3400.
 - [26] V. M. Abazov et al. (D0), Phys. Lett. B **693**, 81 (2010), 1006.3575.

- [27] S. Chatrchyan et al. (CMS), Phys. Rev. Lett. **112**, 171802 (2014), 1312.4194.
- [28] A. M. Sirunyan et al. (CMS), JHEP **07**, 003 (2017), 1702.01404.
- [29] M. Aaboud et al. (ATLAS), JHEP **07**, 176 (2018), 1803.09923.
- [30] G. Aad et al. (ATLAS), Eur. Phys. J. C **76**, 12 (2016), 1508.05796.
- [31] T. Aaltonen et al. (CDF), Phys. Rev. Lett. **101**, 192002 (2008), 0805.2109.
- [32] V. M. Abazov et al. (D0), Phys. Lett. B **701**, 313 (2011), 1103.4574.
- [33] V. Khachatryan et al. (CMS), JHEP **02**, 079 (2017), 1610.04857.
- [34] A. M. Sirunyan et al. (CMS), JHEP **06**, 102 (2018), 1712.02399.
- [35] M. Aaboud et al. (ATLAS), JHEP **05**, 123 (2019), 1812.11568.
- [36] L. Lavoura, Eur. Phys. J. **C29**, 191 (2003), hep-ph/0302221.
- [37] C. Degrande, F. Maltoni, J. Wang, and C. Zhang, Phys. Rev. **D91**, 034024 (2015), 1412.5594.
- [38] G. Durieux, F. Maltoni, and C. Zhang, Phys. Rev. **D91**, 074017 (2015), 1412.7166.
- [39] S. L. Glashow and S. Weinberg, Phys. Rev. **D15**, 1958 (1977).
- [40] E. A. Paschos, Phys. Rev. **D15**, 1966 (1977).
- [41] Q.-H. Cao, B. Yan, J.-H. Yu, and C. Zhang, Chin. Phys. C **41**, 063101 (2017), 1504.03785.
- [42] Q.-H. Cao and B. Yan, Phys. Rev. D **92**, 094018 (2015), 1507.06204.
- [43] Q.-H. Cao, B. Yan, C. Yuan, and Y. Zhang, Phys. Rev. D **102**, 055010 (2020), 2004.02031.
- [44] E. Ma, Phys. Rev. Lett. **81**, 1171 (1998), hep-ph/9805219.
- [45] Q.-H. Cao, S.-L. Chen, E. Ma, B. Yan, and D.-M. Zhang, Phys. Lett. B **779**, 430 (2018), 1707.05896.
- [46] E. Aprile et al. (XENON), JCAP **2011**, 031 (2020), 2007.08796.
- [47] J. Aalbers et al. (DARWIN), JCAP **1611**, 017 (2016), 1606.07001.
- [48] M. Blanke and S. Kast, JHEP **05**, 162 (2017), 1702.08457.
- [49] M. Blanke, S. Das, and S. Kast, JHEP **02**, 105 (2018), 1711.10493.
- [50] S. Bar-Shalom and A. Rajaraman, Phys. Rev. D **77**, 095011 (2008), 0711.3193.
- [51] W. Bernreuther, J. Phys. **G35**, 083001 (2008), 0805.1333.
- [52] M. Linster and R. Ziegler, JHEP **08**, 058 (2018), 1805.07341.
- [53] A. DiFranzo, K. I. Nagao, A. Rajaraman, and T. M. P. Tait, JHEP **11**, 014 (2013), [Erratum: JHEP **01**, 162 (2014)], 1308.2679.
- [54] C. Kilic, M. D. Klimek, and J.-H. Yu, Phys. Rev. **D91**, 054036 (2015), 1501.02202.
- [55] K. A. Mohan, D. Sengupta, T. M. P. Tait, B. Yan, and C. P. Yuan, JHEP **05**, 115 (2019), 1903.05650.
- [56] G. 't Hooft and M. J. G. Veltman, Nucl. Phys. **B153**, 365 (1979).
- [57] T. Hahn and M. Perez-Victoria, Comput. Phys. Commun. **118**, 153 (1999), hep-ph/9807565.
- [58] ATLAS (2013), ATL-PHYS-PUB-2013-012.
- [59] ATLAS (2016), ATL-PHYS-PUB-2016-019.
- [60] Y.-J. Zhang and J.-F. Shen, Eur. Phys. J. **C80**, 811 (2020).
- [61] M. S. Chanowitz, M. A. Furman, and I. Hinchliffe, Nucl. Phys. **B153**, 402 (1979).
- [62] B. W. Lee, C. Quigg, and H. B. Thacker, Phys. Rev. Lett. **38**, 883 (1977).
- [63] B. W. Lee, C. Quigg, and H. B. Thacker, Phys. Rev. **D16**, 1519 (1977).
- [64] M. S. Chanowitz, M. A. Furman, and I. Hinchliffe, Phys. Lett. **78B**, 285 (1978).
- [65] N. Aghanim et al. (Planck) (2018), 1807.06209.
- [66] J. Hisano, K. Ishiwata, and N. Nagata, Phys. Rev. D **82**, 115007 (2010), 1007.2601.
- [67] R. J. Hill and M. P. Solon, Phys. Rev. D **91**, 043504 (2015), 1401.3339.
- [68] V. A. Novikov, M. A. Shifman, A. I. Vainshtein, and V. I. Zakharov, Fortsch. Phys. **32**, 585 (1984).
- [69] R. J. Hill and M. P. Solon, Phys. Rev. D **91**, 043505 (2015), 1409.8290.
- [70] S. Dulat, T.-J. Hou, J. Gao, M. Guzzi, J. Huston, P. Nadolsky, J. Pumplin, C. Schmidt, D. Stump, and C. Yuan, Phys. Rev. D **93**, 033006 (2016), 1506.07443.
- [71] M. Freytsis and Z. Ligeti, Phys. Rev. D **83**, 115009 (2011), 1012.5317.
- [72] C. Amole et al. (PICO), Phys. Rev. **D100**, 022001 (2019), 1902.04031.
- [73] E. Aprile et al. (XENON), Phys. Rev. Lett. **121**, 111302 (2018), 1805.12562.
- [74] A. M. Sirunyan et al. (CMS), JHEP **10**, 244 (2019), 1908.04722.
- [75] G. Aad et al. (ATLAS) (2020), 2010.14293.
- [76] G. Aad et al. (ATLAS), Eur. Phys. J. C **80**, 737 (2020), 2004.14060.
- [77] A. M. Sirunyan et al. (CMS), Eur. Phys. J. C **81**, 3 (2021), 2008.05936.
- [78] J. Alwall, R. Frederix, S. Frixione, V. Hirschi, F. Maltoni, O. Mattelaer, H. S. Shao, T. Stelzer, P. Torrielli, and M. Zaro, JHEP **07**, 079 (2014), 1405.0301.
- [79] T. Sjöstrand, S. Ask, J. R. Christiansen, R. Corke, N. Desai, P. Ilten, S. Mrenna, S. Prestel, C. O. Rasmussen, and P. Z. Skands, Comput. Phys. Commun. **191**, 159 (2015), 1410.3012.
- [80] J. de Favereau, C. Delaere, P. Demin, A. Giammanco, V. Lemaitre, A. Mertens, and M. Selvaggi (DELPHES 3), JHEP **02**, 057 (2014), 1307.6346.
- [81] H. Acaroglu and M. Blanke (2021), 2109.10357.